

Topological One-Way Large-Area Waveguide States in Magnetic Photonic Crystals

Mudi Wang¹, Ruo-Yang Zhang¹, Lei Zhang^{1,2,3}, Dongyang Wang¹, Qinghua Guo^{1,4},
Zhao-Qing Zhang¹ and C. T. Chan^{1,*}

¹*Department of Physics, The Hong Kong University of Science and Technology, Clear Water Bay, Hong Kong 999077, China*

²*State Key Laboratory of Quantum Optics and Quantum Optics Devices, Institute of Laser Spectroscopy, Shanxi University, Taiyuan 030006, China*

³*Collaborative Innovation Center of Extreme Optics, Shanxi University, Taiyuan 030006, China*

⁴*Institute for Advanced Study, The Hong Kong University of Science and Technology, Clear Water Bay, Hong Kong 999077, China*

 (Received 8 August 2020; accepted 14 January 2021; published 9 February 2021)

We have theoretically and experimentally achieved large-area one-way transport by using heterostructures consisting of a domain of an ordinary photonic crystal sandwiched between two domains of magnetic photonic crystals. The nonmagnetized domain carries two orthogonal one-way waveguide states which have amplitude uniformly distributed over a large area. We show that such one-way waveguide states can be used to abruptly narrow the beam width of an extended state to concentrate energy, and the transport is robust against different kinds of defects and imperfections. They are also immune to the Anderson-type localization when large randomness is introduced.

DOI: [10.1103/PhysRevLett.126.067401](https://doi.org/10.1103/PhysRevLett.126.067401)

Topological physics [1–40] is flourishing as a very exciting field, which has drawn attention in both fundamental research and applied science. Topological materials, either insulators [1–33] or those which are gapless [34–38], all commonly feature the striking phenomenon of topological boundary transport, exhibiting edge states or surface states that are robust against disorder. Among them, one of the most striking examples is the one-way transport in quantum Hall systems [9–14], in which the magnetic field breaks time-reversal symmetry (TRS) and produces quantized Hall conductance. Its quantization is a topological phenomenon and is connected with an integer Chern number in the associated Landau bands. In a finite system, a nonzero Chern number also gives rise to one-way edge modes. Their counterparts in classical wave systems have also been reported in both theoretical [15–19] and experimental [20–24] research. However, topological principles can guarantee the existence of only a certain number of transport channels [39,40]. How well or how fast (group velocity) those channels can transport information or energy depends on the structural details. It is highly desirable if the transport characteristics of topological modes can be controlled.

A photonic crystal (PC) carrying Dirac points with a zero Chern number is topologically trivial. The transport of an electromagnetic (EM) wave can be blocked by defects or disorder. Here, we show that when such a PC is sandwiched [25,26] between two topological crystals in which TRS is broken by two oppositely biased magnetic fields, the topologically trivial PC can exhibit unidirectional transmission that is robust to imperfections and defects. This type of heterostructure is collectively a topologically

nontrivial system and permits one-way transport of waves in a large area, which has some advantages over topological edge modes [15–24,31–33], where the wave energy is confined in a narrow boundary. For example, topological one-way beam spatial collimation can be easily achieved, and we have a large area to collect incident wave energy and many degrees of freedom to control wave impedance.

The heterostructure consists of three domains, labeled as *A*, *B*, and *C* by three different colors, as shown in Fig. 1(a). Each domain is made up of a hexagonal array (16 mm lattice constant) of cylindrical yttrium iron garnet (YIG) rods (4 mm diameter, 10 mm height). The YIG rods are magnetized by an external magnetic field along the positive (negative) vertical direction in domain *A* (*C*), and no magnetic field is imposed in domain *B*. The detailed experimental setup is given in Supplemental Material [41]. The band structures of each domain, calculated using COMSOL, are shown in Fig. 1(b). The bulk bands of interest here are the 2D transverse-magnetic (TM) modes. The PC in domain *B* possesses Dirac points at the *K* and *K'* points. Because of TRS breaking imposed by the external field, the Dirac points in domains *A* and *C* become gapped, while domains *A* and *C* carry opposite gap Chern numbers in their second band gap. Since domain *B* is not gapped, an EM wave can propagate inside the band gap (around 11.9 GHz) of domains *A* and *C*; but on its own, the propagation does not display any topological behavior. As domain *B* forms a domain wall separating two topologically distinct domains *A* and *C*, the principle of bulk-edge correspondence [39,40] implies that the combination of *A*, *B*, and *C* domains can give rise to new topologically nontrivial signatures inside

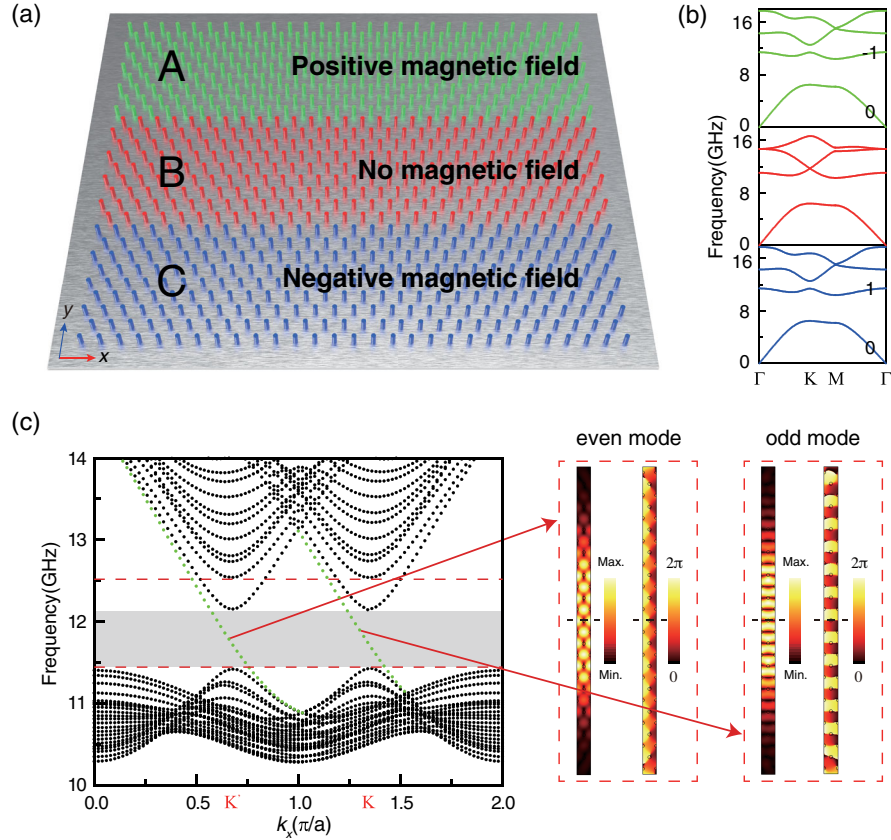


FIG. 1. (a) The schematic picture of the $A|B_9|C$ heterostructure. A positive (negative) magnetic field is added in domain A (C), and no magnetic field is added in domain B. (b) Bulk band structures for A, B, and C, respectively. The Chern numbers of the first and second bands of A and C are marked. (c) Left panel: the projected band structure for $A|B_9|C$. The shadowed area marks the frequency range of the TOLWSs, which are indicated by two green dotted lines. The area between two red dashed lines is the range of bulk gap for A and C. Right panel: the intensity and phase distributions of electric fields of two TOLWSs in domain B, respectively. The black dashed lines are the mirrors.

domain B with the number of unidirectional modes determined by the difference of gap Chern numbers in domains A and C. The projected band structure of the whole heterostructure is shown in Fig. 1(c). There are two (one is even and the other is odd about the $y = 0$ plane) topological one-way large-area waveguide states (TOLWSs) in the bulk gap, which are uniformly extended in the whole domain B, as shown in the right panel in Fig. 1(c) by the intensity and phase distributions of the electric field. We note that only two waveguide states with a topological one-way property exist in the shadow area in Fig. 1(c), which is very different with the usual broad waveguides [42,43] with characteristic features of carrying numerous bands and flattening dispersion when Littrow reflection dominates. The presence of a Dirac cone in domain B is crucial. If replaced by air or a uniform medium that does not carry a Dirac cone, no TOLWSs will exist as shown in Fig. S1 [41]. The one-way mode is distributed evenly over a large area, which is not a local magnetic field effect, and, hence, the channel can carry a gigantic amount of energy without burning the device, in contrast to the edge modes in other one-way structures [15–24,31–33] which are spatially tightly confined.

Figure 2(a) shows the photo of the sample $A|B_9|C$. The subscript “9” indicates that the nonmagnetized domain B has nine layers in the y direction. We can selectively excite the even or odd waveguide mode in domain B by polarized sources (see Fig. S2 [41]). These two waveguide modes with different symmetries have the large separation in momentum space. The EM waves are injected into the sample at the point source labeled by a magenta star on the right boundary. The dispersion of each TOLWS can be obtained by measuring the field scanned along the direction at different frequencies and then performing a Fourier transform. The experimental results are plotted using color maps in Figs. 2(b) and 2(c) for the even and odd modes, respectively. We find good agreements with the numerical results marked by the green lines.

It is remarkable that domain B acquires the property of unidirectional transmission in a certain frequency range, when sandwiched between domains A and C. An EM field can pass through the bulk of domain B when a point source (odd mode at 11.9 GHz) is placed on the right boundary, as shown in Fig. 3(a). However, transmission is forbidden for the same $A|B_9|C$ configuration when the point source is located on the left boundary as shown in Fig. 3(b). Strong

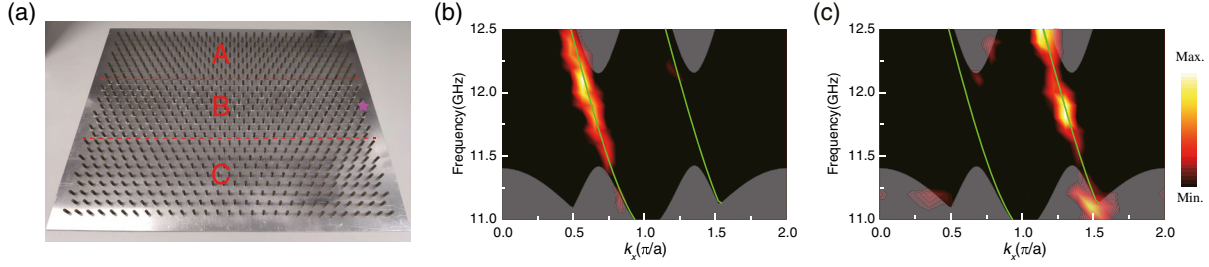


FIG. 2. (a) The photo of the $A|B_9|C$ sample. The magenta star marks the position of the point source. (b),(c) The selective excitations of the even (b) and odd (c) TOLWSs by the corresponding point dipolar sources. The color map is the experimental result, while the gray area and the green lines are the calculated results.

transmission asymmetry is also observed at other passing frequencies of the TOLWSs, which is shown by the shadowed region in Fig. 3(d), where S_{21} and S_{12} denote the measured transmission spectra averaged along the direction for the two cases. Figure 3(e) shows the transmitted amplitude measured point by point along the white dotted lines 1 and 2 in Figs. 3(a) and 3(b) for these two cases. These results provide strong evidence of one-way transport in such heterostructures.

The TOLWS here has a much larger and tunable transmission area than an ordinary topological one-way edge mode [15–24] or antichiral edge states [31–33], which are exponentially confined to the boundary. Taking advantage of these characteristics, we can achieve topological one-way beam spatial collimation using the structure shown in Fig. 3(c), in which the layer number in domain B is sharply

reduced from 9 to 0 (from the right side to the left side). If there were no topological protection, the waves would have been strongly reflected when the transport channel is abruptly narrowed. However, the absence of backscattering channels [as evident from Fig. 1(c)] forces the waves to go forward, and all the energy is squeezed from the wide channel into the narrow channel. The simulation result of topological one-way beam spatial collimation effect is shown in Fig. 3(c), where an extended TOLWS excited by a point source on the right is collimated into a narrow channel on the left due to the sudden narrowing of the transport channel. Figure 3(f) compares the intensity of the waves along the white dotted lines 3 [Fig. 3(c)] and 1 [Fig. 3(a)], showing that the intensity in the narrow channel is significantly increased. The wide and tunable width of TOLWSs allows for a high-efficiency collection of

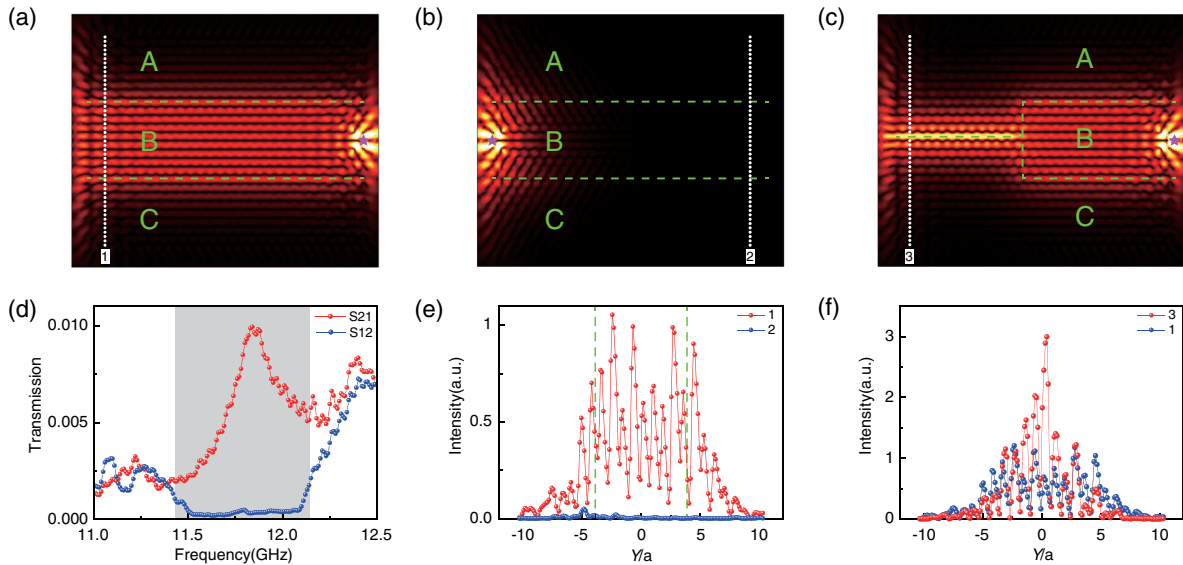


FIG. 3. (a),(b) Simulated electric field intensity distributions of excited by point sources (magenta stars) on the right and left sides for the same $A|B_9|C$ configurations at 11.9 GHz, respectively. (c) Simulated electric field intensity distribution using a point source excitation at 11.9 GHz on the right boundary of the B domain. Its width is sharply reduced from nine layers to 0. (d) S_{21} (S_{12}) is the measured transmission spectrum averaged along the transverse direction in the B domain when the point source is placed on the right (left) boundary. (e) The red (blue) solid line is the experimental intensity profiles at 11.9 GHz along the white dotted line 1 (2) in (a) [(b)]. The area between two green dashed lines represents domain B . (f) The red (blue) solid line shows the experimentally measured intensity profiles along the white dotted line 3 (1) in (c) [(a)].

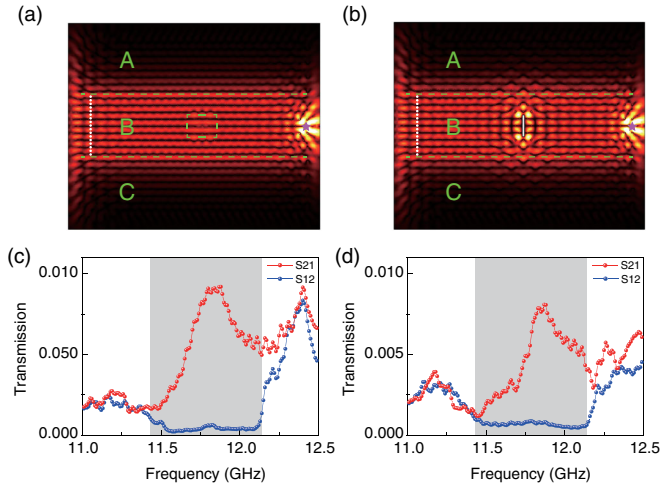


FIG. 4. (a),(b) Simulated electric field intensity distributions at 11.9 GHz in the heterostructures with a void defect, in which ten unit cells are removed inside the green dashed rectangle and a PEC obstacle, respectively. (c),(d) Measured average transmission spectra S_{21} and S_{12} in domain B for the void and PEC defects, respectively.

energy from an extended region and guides all the captured energy into a narrow channel.

Next, we show the robustness of TOLWS transport against various kinds of defect and randomness. In Figs. 4(a) and 4(b), we create a void in the middle of the B domain by removing ten unit cells as marked by the green dashed rectangle and a PEC obstacle, respectively, and the point sources (exciting the odd mode) are used to excite the TOLWSs. The simulation results of electric field

intensity distribution at 11.9 GHz show almost complete recovery of the TOLWS after passing through the area with the void or PEC obstacle, which appear almost identical to that shown in Fig. 3(a) without defects, indicating that the void or PEC obstacle is almost invisible to the TOLWS. Remarkably, inside the passing frequency window of the TOLWSs, as shown in Figs. 4(c) and 4(d), the spectra of average transmission S_{21} and S_{12} are also found to be nearly identical to those shown in Fig. 3(d) without defects. The robustness of the one-way transport of the TOLWSs is a result of TRS breaking in domains A and C , which is very different from the valley transport produced by parity breaking [25–30], in which the transport can be greatly compromised by defects due to the presence of a back-scattering channel.

Now we study the transport of TOLWSs in the presence of randomness in domain B . It is well known that all EM waves will be localized in random two-dimensional systems due to Anderson localization [44–49]. The localization effect is demonstrated in the four upper panels in Fig. 5(a) at the frequency of 11.7 GHz. The first panel shows the perfect transmission for an ordered PC, and the other three panels show the complete blocking of waves by the three different random configurations of the YIG rods inside the PC. Here, randomness is introduced inside the green rectangle by randomly assigning the permittivity of YIG rods between 1 and 26.6. However, if domain B is sandwiched by domains A and C as shown in Fig. 1(a), the transport of TOLWSs cannot be hindered by the presence of defects or randomness due to the absence of a back-scattering channel and the accompanying coherent back-scattering effect. The simulation results of the transport of

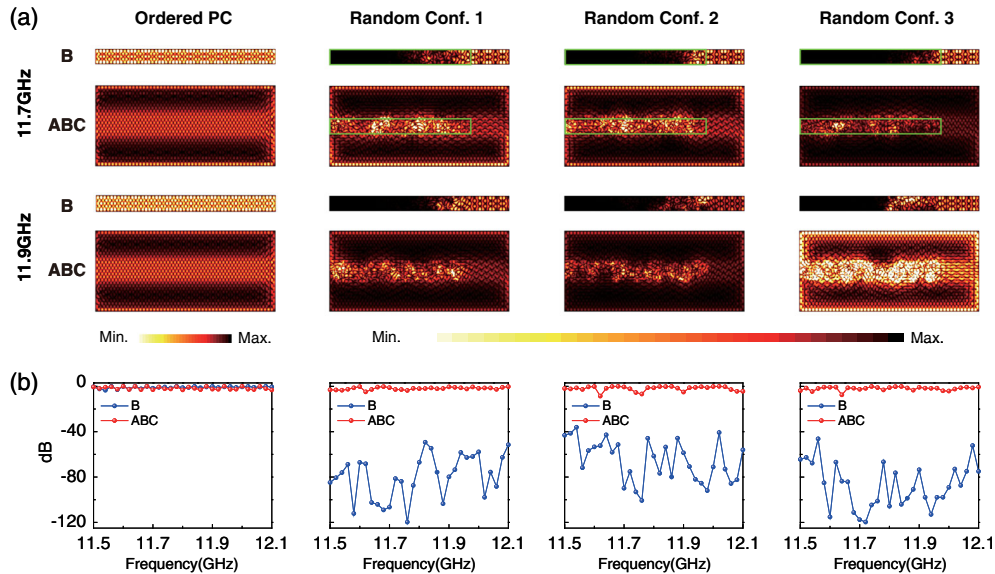


FIG. 5. (a) The simulations of a crystal B_5 and heterostructures $A|B_5|C$ in the ordered PC and three different configurations of random PCs, in which the permittivity of YIG rods inside the green rectangle is randomly selected between 1 and 26.6. Electromagnetic waves are incident from the right. (b) The corresponding transmission spectra for B_5 and heterostructures $A|B_5|C$.

TOLWS at 11.7 GHz are shown in the second-row panels in Fig. 5(a). In the case of no randomness, the first panel shows again the perfect transmission with uniform field distribution inside the B domain. When randomness is introduced, the other three panels show the irregular field distributions inside the B domain. However, the transport of waves is protected with an average transmission close to unity. Similar results are shown for the case of 11.9 GHz. In Fig. 5(b), we plot the average transmission spectra in log scale for both the ordered case and the three random cases. Close to unity, transmission is found in the heterostructure ABC systems for all three random cases. It should be pointed out that the randomness shown in Fig. 5(b) is significantly higher than the smallest randomness that can block all the transmission inside the gap of the disordered B_5 as shown in Fig. S3 [41].

Such robustness can be understood from the formation of TOLWSs. The application of two oppositely biased magnetic fields in domains A and C will introduce one-way interface states at the interfaces of AB and BC in the same direction. As domain B itself does not have a gap, the two topological interface states (one from A and one from C) do not decay inside domain B , and they couple strongly and hybridize into a pair of even-odd waveguide states with almost uniform field amplitude inside the waveguide. Thus, the pair of waveguide states owes their topological properties to the Chern numbers in domains A and C , even though domain B is topologically trivial. It can be viewed as a form of proximity effect, but, oddly, domain B (the width of the waveguide) can be as big as one likes, at the expense of a smaller operational bandwidth for one-way transport. We note again that the merging of two interface states into waveguide states does not depend on the width of the B domain. This is demonstrated in Fig. S4 [41] as the number of layers in B is increased to 91 rows.

In conclusion, we have realized and experimentally observed the TOLWSs by designing heterostructures using magnetic PCs. The TOLWSs cover a large area and, hence, have more degrees of freedom to tune energy transport capacity and characteristics. As a result, unique topological one-way beam spatial collimation effect is demonstrated. As TRS is broken in this system, the ABC structure is robust to different kinds of defect and randomness. Since the waveguide can be as wide as we like, it also provides an efficient way to collect information and energy. A similar phenomenon may also be found in electronic and phononic systems.

This work was supported by the Hong Kong Research Grants Council under Grants No. AoE/P-02/12 and No. 16303119. L. Z. was supported by National Natural Science Foundation of China Grant No. 12074230, National Key R&D Program of China under Grants No. 2017YFA0304203 and No. 1331KSC, Shanxi Province 100-Plan Talent Program. We thank Professor Xu-Lin Zhang for helpful discussions.

*Corresponding author.

phchan@ust.hk

- [1] M. Rechtsman, J. Zeuner, Y. Plotnik, Y. Lumer, D. Podolsky, F. Dreisow, S. Nolte, M. Segev, and A. Szameit, Photonic Floquet topological insulators, *Nature (London)* **496**, 196 (2013).
- [2] M. Atala, M. Aidelsburger, J. Barreiro, D. Abanin, T. Kitagawa, E. Demler, and I. Bloch, Direct measurement of the Zak phase in topological Bloch bands, *Nat. Phys.* **9**, 795 (2013).
- [3] R. Süsstrunk and S. Huber, Observation of phononic helical edge states in a mechanical topological insulator, *Science* **349**, 47 (2015).
- [4] S. Mukherjee and M. Rechtsman, Observation of Floquet solitons in a topological bandgap, *Science* **368**, 856 (2020).
- [5] G. Harari *et al.* Topological insulator laser: Theory, *Science* **359**, eaar4003 (2018).
- [6] M. Bandres *et al.* Topological insulator laser: Experiments, *Science* **359**, eaar4005 (2018).
- [7] S. Barik, A. Karasahin, C. Flower, T. Cai, H. Miyake, W. DeGottardi, M. Hafezi, and E. Waks A topological quantum optics interface., *Science* **359**, 666 (2018).
- [8] M. Parto, S. Wittek, H. Hodaei, G. Harari, M. A. Bandres, J. Ren, M. C. Rechtsman, M. Segev, D. N. Christodoulides, and M. Khajavikhan, Edge-Mode Lasing in 1D Topological Active Arrays, *Phys. Rev. Lett.* **120**, 113901 (2018).
- [9] K. v. Klitzing, G. Dorda, and M. Pepper, New Method for High-Accuracy Determination of the Fine-Structure Constant Based on Quantized Hall Resistance, *Phys. Rev. Lett.* **45**, 494 (1980).
- [10] D. C. Tsui, H. L. Stormer, and A. C. Gossard, Two-Dimensional Magnetotransport in the Extreme Quantum Limit, *Phys. Rev. Lett.* **48**, 1559 (1982).
- [11] M. Kohmoto, Topological invariant and the quantization of the Hall conductance, *Ann. Phys. (N.Y.)* **160**, 343 (1985).
- [12] K. v. Klitzing, The quantized Hall effect, *Rev. Mod. Phys.* **58**, 519 (1986).
- [13] K. S. Novoselov, A. K. Geim, S. V. Morozov, D. Jiang, M. I. Katsnelson, I. V. Grigorieva, S. V. Dubonos, and A. A. Firsov, Two-dimensional gas of massless Dirac fermions in graphene, *Nature (London)* **438**, 197 (2005).
- [14] Y. Zhang, Y.-W. Tan, H. L. Stormer, and P. Kim, Experimental observation of the quantum Hall effect and Berry's phase in graphene, *Nature (London)* **438**, 201 (2005).
- [15] F. D. M. Haldane and S. Raghu, Possible Realization of Directional Optical Waveguides in Photonic Crystals with Broken Time-Reversal Symmetry, *Phys. Rev. Lett.* **100**, 013904 (2008).
- [16] S. Raghu and F. D. M. Haldane, Analogs of quantum-Hall-effect edge states in photonic crystals, *Phys. Rev. A* **78**, 033834 (2008).
- [17] Z. Wang, Y. D. Chong, J. D. Joannopoulos, and M. Soljacic, Reflection-Free One-Way Edge Modes in a Gyromagnetic Photonic Crystal, *Phys. Rev. Lett.* **100**, 013905 (2008).
- [18] K. Fang, Z. Yu, and S. Fan, Realizing effective magnetic field for photons by controlling the phase of dynamic modulation, *Nat. Photonics* **6**, 782 (2012).
- [19] Z. Yang, F. Gao, X. Shi, X. Lin, Z. Gao, Y. Chong, and B. Zhang, Topological Acoustics, *Phys. Rev. Lett.* **114**, 114301 (2015).

- [20] Z. Wang, Y. Chong, J. D. Joannopoulos, and M. Soljacic, Observation of unidirectional backscattering-immune topological electromagnetic states, *Nature (London)* **461**, 772 (2009).
- [21] Y. Poo, R. X. Wu, Z. F. Lin, Y. Yang, and C. T. Chan, Experimental Realization of Self-Guiding Unidirectional Electromagnetic Edge States, *Phys. Rev. Lett.* **106**, 093903 (2011).
- [22] M. Hafezi, S. Mittal, J. Fan, A. Migdall, and J. M. Taylor, Imaging topological edge states in silicon photonics, *Nat. Photonics* **7**, 1001 (2013).
- [23] L. Lu, J. D. Joannopoulos, and M. Soljacic, Topological photonics, *Nat. Photonics* **8**, 821 (2014).
- [24] Y. Ding, Y. Peng, Y. Zhu, X. Fan, J. Yang, B. Liang, X. Zhu, X. Wan, and J. Cheng, Experimental Demonstration of Acoustic Chern Insulators, *Phys. Rev. Lett.* **122**, 014302 (2019).
- [25] S. G. Cheng, J. J. Zhou, H. Jiang, and Q.-F. Sun, The valley filter efficiency of monolayer graphene and bilayer graphene line defect model, *New J. Phys.* **18**, 103024 (2016).
- [26] M. Wang, W. Zhou, L. Bi, C. Qiu, M. Ke, and Z. Liu, Valley-locked waveguide transport in acoustic heterostructures, *Nat. Commun.* **11**, 3000 (2020).
- [27] J. Lu, C. Qiu, L. Ye, X. Fan, M. Ke, F. Zhang, and Z. Liu, Observation of topological valley transport of sound in sonic crystals, *Nat. Phys.* **13**, 369 (2017).
- [28] M. Wang, L. Ye, J. Christensen, and Z. Liu, Valley Physics in Non-Hermitian Artificial Acoustic Boron Nitride, *Phys. Rev. Lett.* **120**, 246601 (2018).
- [29] J.-W. Dong, X.-D. Chen, H. Zhu, Y. Wang, and X. Zhang, Valley photonic crystals for control of spin and topology, *Nat. Mater.* **16**, 298 (2017).
- [30] X.-T. He, E.-T. Liang, J.-J. Yuan, H.-Y. Qiu, X.-D. Chen, F.-L. Zhao, and J.-W. Dong, A silicon-on-insulator slab for topological valley transport, *Nat. Commun.* **10**, 1 (2019).
- [31] E. Colomes and M. Franz, Antichiral Edge States in a Modified Haldane Nanoribbon, *Phys. Rev. Lett.* **120**, 086603 (2018).
- [32] Y. Yang, D. Zhu, Z. H. Hang, and Y. D. Chong, Observation of antichiral edge states in a circuit lattice, *arXiv*: 2008.10161.
- [33] P. Zhou, G. G. Liu, Y. Yang, Y.-H. Hu, S. Ma, H. Xue, Q. Wang, L. Deng, and B. Zhang, Observation of Photonic Antichiral Edge States, *Phys. Rev. Lett.* **125**, 263603 (2020).
- [34] L. Lu, Z. Wang, D. Ye, L. Ran, L. Fu, J. D. Joannopoulos, and M. Soljačić, Experimental observation of Weyl points, *Science* **349**, 622 (2015).
- [35] W.-J. Chen, M. Xiao, and C. T. Chan, Phononic crystals possessing multiple Weyl points and the experimental observation of robust surface states, *Nat. Commun.* **7**, 13038 (2016).
- [36] H. He, C. Qiu, L. Ye, X. Cai, X. Fan, M. Ke, F. Zhang, and Z. Liu, Topological negative refraction of surface acoustic waves in a Weyl phononic crystal, *Nature (London)* **560**, 61 (2018).
- [37] B. Yang *et al.*, Ideal Weyl points and helicoid surface states in artificial photonic crystal structures, *Science* **359**, 1013 (2018).
- [38] Q. Guo, O. You, B. Yang, J. B. Sellman, E. Blythe, H. Liu, Y. Xiang, J. Li, D. Fan, J. Chen, C. T. Chan, and S. Zhang, Observation of Three-Dimensional Photonic Dirac Points and Spin-Polarized Surface Arcs, *Phys. Rev. Lett.* **122**, 203903 (2019).
- [39] Y. Hatsugai, Chern Number and Edge States in the Integer Quantum Hall Effect, *Phys. Rev. Lett.* **71**, 3697 (1993).
- [40] C.-K. Chiu, J. C. Y. Teo, A. P. Schnyder, and S. Ryu, Classification of topological quantum matter with symmetries, *Rev. Mod. Phys.* **88**, 035005 (2016).
- [41] See Supplemental Material at <http://link.aps.org/supplemental/10.1103/PhysRevLett.126.067401> for the experimental methods.
- [42] H. Benisty, N. Piskunov, P. K. Kashkarov, and O. Khayam, Crossing of manifolds leads to flat dispersion: Blazed Littrow waveguides, *Phys. Rev. A* **84**, 063825 (2011).
- [43] H. Benisty and N. Piskunov, Mastered dispersion of material resonators: Broad corrugated waveguides working under the Littrow regime, *Appl. Phys. Lett.* **102**, 151107 (2013).
- [44] P. A. Lee and D. S. Fisher, Anderson Localization in Two Dimensions, *Phys. Rev. Lett.* **47**, 882 (1981).
- [45] S. Fishman, D. R. Grempel, and R. E. Prange, Chaos, Quantum Recurrences, and Anderson Localization, *Phys. Rev. Lett.* **49**, 509 (1982).
- [46] T. Schwartz, G. Bartal, S. Fishman, and M. Segev, Transport and Anderson localization in disordered two-dimensional photonic lattices, *Nature (London)* **446**, 52 (2007).
- [47] G. Roati, C. D'Errico, L. Fallani, M. Fattori, C. Fort, M. Zaccanti, G. Modugno, M. Modugno, and M. Inguscio, Anderson localization of a non-interacting Bose-Einstein condensate, *Nature (London)* **453**, 895 (2008).
- [48] S. Faez, A. Strybulevych, J. H. Page, A. Lagendijk, and B. A. van Tiggelen, Observation of Multifractality in Anderson Localization of Ultrasound, *Phys. Rev. Lett.* **103**, 155703 (2009).
- [49] M. Segev, Y. Silberberg, and D. N. Christodoulides, Anderson localization of light, *Nat. Photonics* **7**, 197 (2013).